This is a peer-reviewed, accepted author manuscript of the following conference paper: Higgins, M, Jones, CE, Peña Alzola, R & Burt, G 2024, 'Low frequency design criteria for carbon fibre composite casings for aircraft power electronic converters', Paper presented at International Conference on More Electric Aircraft, Toulouse, France, 7/02/24 - 8/02/24.

Low frequency Design Criteria for Carbon Fibre Composite Casings for Aircraft Power Electronic Converters

Mark Higgins (1), Catherine E. Jones (2), Rafael Peña Alzola (3), Graeme Burt (4)
1 : University of Strathclyde, 16 Richmond Street, Glasgow, m.higgins.2016@uni.strath.ac.uk
2 : University of Strathclyde, catherine.e.jones@strath.ac.uk 3 : University of Strathclyde, rafael.pena-alzola@strath.ac.uk 4 : University of Strathclyde, Graeme.burt@strath.ac.uk

Abstract
Two key technologies supporting decarbonisation of aviation are the light-weighting of aircraft structures, and the electrification of on-board power and propulsion systems. Achieving the target high power densities required for electrical power system equipment, including power electronic converters (PEC) is extremely challenging. A modularised electrical power system (EPS) which exploits the use of carbon fibre reinforced polymer (CFRP), rather than aluminium, for non-electrically active components (e.g., casings) for EPS equipment offers an opportunity for more compact, lightweight equipment design. However, existing knowledge of the electrical response of CFRP at a component scale, and how this impacts on the design of systems where electrical and structural systems interact, is limited.

This paper provides a set of low frequency (<200 kHz), component scale models of a quasi-isotropic layup of CFRP, suitable for use with a behavioural simulation model of a 6-switch inverter to investigate the influence of casing on fault response, and enable capture of design criteria for resilient, low frequency design of CFRP casings for PECs. This includes investigation of key design interdependencies including influence of CFRP layup, design of electrical bonding points and interdependencies with wider system design considerations, including protection strategies.

Introduction

Electrification of power and propulsion systems is a key technology for the decarbonisation of aviation. A barrier to realising the electrical power systems (EPS) needed for these new propulsion systems, are the high-power densities required for the EPS equipment. This includes power electronic converters (PEC), which are critical for the regulation of voltage and frequency levels, and control of power flow. The power density of PECs for aircraft applications is currently ~12 kW/kg [1]. However, power densities of ~40 kW/kg [2] are needed to meet electrification targets for aerospace. PEC will contribute a significant weight to the EPS for these new, electrified propulsion systems. For example, it is estimated that PECs will contribute ~20% of EPS weight for an all-electric aircraft with fuel cells as a power source [2]. Around 19% of the weight of a PEC module is attributable to the aluminium casing and heat sink [3]. other notable components contributing to the weight of the module are the filters housed within the enclosure, which attribute to around 43% of the weight [4]. Replacement of all, or part, of the aluminium casing with CFRP offers a route (in tandem with other technology advances, such as wide bandgap solid state switches) to improve power density. To design these CFRP based casings, electrical models of the CFRP are needed to carry out system design trades.

CFRP is ~30% less dense than aluminium, and is established structural material for lighter weight structures on aircraft. As such, more than 50% of structures on state-of-the-art aircraft made from CFRP [5], reducing the total structural weight of the aircraft by ~20% [6]. CFRP is comprised of carbon fibres (an electrical conductor) held in place by a polymer resin (an electrical insulator). This results in an electrically complex, heterogeneous material, with an electrical conductivity which is ~1000 times lower than that of aluminium [7]. If CFRP is to form the casing for a PEC, then it is necessary to understand how the CFRP casing will interact electrically with PEC. The role of the casing on a PEC is to provide appropriate levels of electromagnetic shielding, and to adhere to industry standards for radiated emissions (for aerospace, DO-160 [8]). The casing will also provide a pathway to ground for fault current. Hence the electrical design of the CFRP casing must consider higher frequency (>GHz) (EM shielding

functionality) and lower frequency (<MHz) (fault current conduction capability). The focus of this paper is the design of the casing for low frequency electrical interactions under fault conditions.

Figure 1 and Figure 2 show an example topology for a sub-system in an aircraft EPS, with a PEC unit supplying a motor. The PEC has a CFRP casing. Knowledge of the electrical properties of a CFRP casing at low frequencies are needed to understand failure conditions, and subsequently inform the approach to fault management, for the scenario where electrical fault current may flow through the CFRP casing. An electrical model of CFRP which can be integrated with a behavioural level model [9] of sub-system of an aero-electrical power system is needed, to enable assessment of the response of the EPS sub-system to an electrical fault through the CFRP. Further, such a model enables the sensitivity of the CFRP impedance to different system parameters to be investigated, such that the system can be tuned to give a particular fault response. This includes design decisions on location, size and number of electrical bonding points between the casing and ground, layup of the CFRP casing, and the likely location and nature of the electrical fault current injection into the CFRP.

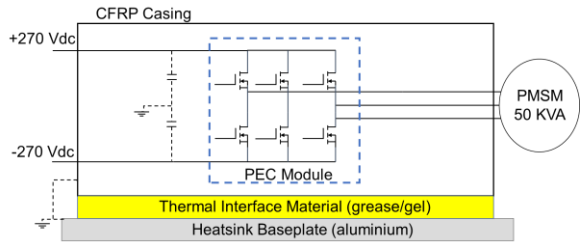

Figure 1: Functionality of PEC casing

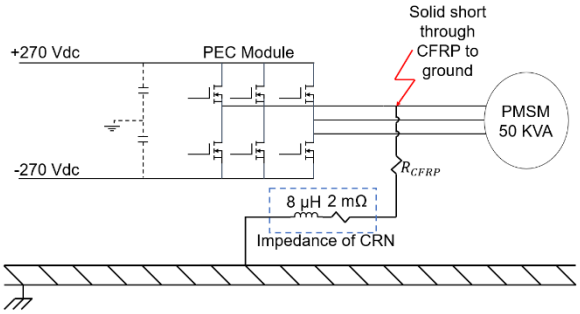

Figure 2: AC rail to ground fault through CFRP investigation

This paper is focussed on a pre-preg non-woven, quasi-isotropic (QI) (fibres oriented at 0°, 90°, +45° and -45°) lay-up of CFRP. The electrical behaviour of CFRP is extremely anisotropic, as the epoxy resin is an electrical insulator, but the carbon fibre is an electrical conductor. The carbon fibres are wavy and therefore create fibre-to-fibre contact points both between fibres lying parallel in the same ply, and between plies. These contact points are randomly distributed across a CFRP component. Where fibres touch, an electrical connection between those fibres is formed. This affects electrical behaviour and increases the challenge of modelling the electrical properties of CFRP [10].

In the literature, several low frequency models of CFRP are based on numerical methods, in which either the influence of variation of the macro-scale resistance in different sections of the conducting pathway is not considered [7, 11], or the level of fidelity is too high to integrate with a sub-system model of a PEC and electrical motor [11-13]. Several models of UD [0°] layups at component scale are presented in the literature, for example [14-16]. A methodology to capture the relationship between resistance and component dimensions is presented in [16]. However, although UD [0°] provides a good starting point to understand the electrical behaviour of CFRP, this layup has limited mechanical properties, and is not representative of a layup that would be used in reality. Further, in these studies, the impact of varying the entry or exit electrode size is not considered.

Lumped impedance models, where the variation in resistance over the conducting pathway is incorporated into the model, are presented in [14, 15]. The advantage of the lumped impedance model, is first that it is at a level of fidelity which can be integrated with a behavioural level simulation model. Second it breaks down the pathway taken by the electrical current through the CFRP into sections, enabling an informed investigation of the influence of each section on the electrical and thermal response of the CFRP, and impact on the fault response of the wider electrical power system. Such a lumped impedance model can then be integrated with a simulation model of a sub-system, to investigate electrical behaviour during both DC and AC rail to ground faults through the CFRP casing, as shown in Figure 2. This will inform the sensitivity requirements

of the protection system, to enable the determination of a set of design criteria for the low-frequency design of CFRP casings for PECs for aircraft applications.

This paper will present a set of experimentally validated, lumped impedance models for a QI layup of CFRP which can be integrated into simulation studies to investigate the fault response for AC and DC rail to ground faults through the CFRP casing, to enable system design trades to take place. Hence, the rest of this paper is structured as follows: Section 1 provides an overview of the experimental method to capture model parameters; Section 2 presents the lumped impedance models developed for a QI layup; Section 3 investigates methods to manipulate fault resistance; Section 4 utilises the model to carry out system design trades. Conclusions and future work are then presented.

1. Capture of parameters for lumped impedance model.

The resistance of a section of a material is given by:

$$\boldsymbol{R = \frac{L}{\sigma A}} \qquad (1),$$

where R (Ω) is the electrical resistance, L (m) the distance between the electrodes, σ (S/m) the electrical conductivity and A (m^2) the cross-sectional area. Hence electrical resistance can be increased by increasing L, decreasing A or σ. Therefore if the pathway taken by electrical current through CFRP is modelled as a lumped resistance, Figure 3, there are discrete resistances attributable to the entry and exit points, R_{entry} (Ω) and R_{exit} (Ω) due to the smaller cross-sectional conducting area at the electrodes, compared to the conducting section of CFRP between electrodes, $R(l_{x,y})$ (Ω), where current is not constrained to conduct through a small cross-sectional area.

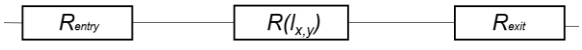

Figure 3: Baseline lumped resistance model

With reference to Figure 3, for the case of an electrical fault through CFRP, the entry resistance, R_{entry}, is the resistance where the fault current first enters the CFRP, and the exit resistance, R_{exit}, will be the exit point where the casing is electrically bonded to ground. The resistance of the pathway between these two points is represented by $R(l_{x,y})$.

The aerospace grade QI layup selected for the model had a layup of MTM44-1 unidirectional prepreg with a stacking sequence of [0°, 90°, +45°, -45°]2S. The volume fraction of carbon fibre was 57%. The fibres laid at 0° and 90° offer stiffness; the fibres laid at +/- 45° offer tensile strength. The panel used for the experiments was 530 x 530 x 4mm. This thickness corresponded to 16 plies. The CFRP panel used in the experiments is shown in Figure 4.

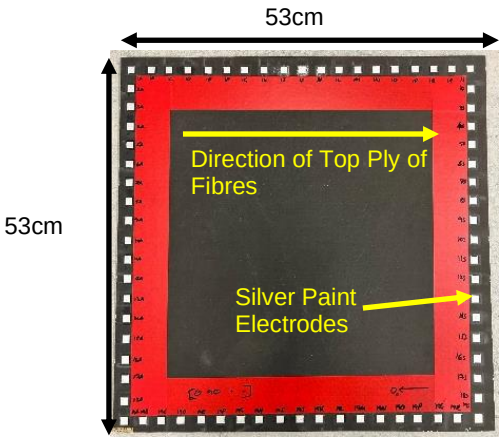

Figure 4: QI CFRP Sample for Electrical Characterization

In order to capture the parameters for the lumped impedance model, a total of 19 electrodes were placed along each edge of the CFRP panel as shown in Figure 4, each separated by a distance of 17.5 mm. This enabled capture of the variation of resistance with distance aligned and perpendicular to the orientation of fibres in the surface ply. Initial electrode size was set to be 10mm x 10mm, corresponding to minimum surface area of an electrical bonding point to ground for aircraft, as outlined in SAE-ARP-1870 [17].

Electrodes were prepared by following the method outlined in [18], by sanding the surface with 150 grit sandpaper to remove the outer layer of epoxy to expose carbon fibres. Silver paint was applied to minimise contact resistance. Copper foil was clamped onto each electrode, and 4-point measurement probes clipped to the foil. Prior to the development of the lumped impedance models for

the CFRP layup, the frequency at which the CFRP exhibits a reactive component towards the total impedance was measured. This was achieved by performing a frequency sweep with a Bode analyser. The results of this test are shown in Figure 5.

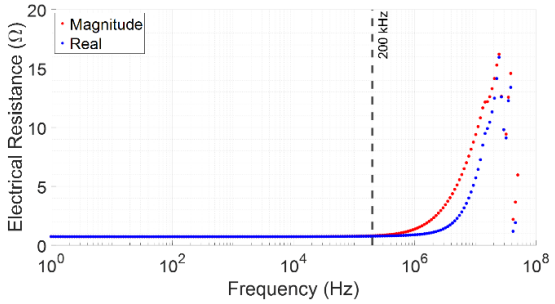

Figure 5: Frequency response of CFRP

By inspection of Figure 5, for frequencies below ~200 kHz the CFRP exhibits a purely resistive behaviour: the magnitude and real part of the impedance are equal, and there is no reactive component. Above 200 kHz the magnitude and real part of the impedance begin to diverge, and the CFRP exhibits an inductive behaviour. The switching frequency for the PEC that has been used for the evaluation of failure scenarios has a switching frequency of 25 kHz. Hence it can be assumed that the impedance of the CFRP to a fault current can be modelled as a lumped, resistance model, with impedances measured at DC valid up to ~200 kHz.

While there are industry standards for the cross-sectional area of an electrical bonding point, the entry point may be much smaller if due to abrasion from a chaffed wire and injection of a fault current [15]. By inspection of (1), this smaller cross-sectional area will impact on resistance at the injection site. Hence, a second set of experiments were run to investigate influence of cross-sectional area on resistance.

Existing industry standards require the electrical resistance of each bonding point must be no more than 2.5 mΩ (SAE-ARP-1870) [17], The minimum number of bonding points is not defined in the standards as this is decided by the designers of the equipment. Typically, the casing would be grounded at multiple locations for safety purposes [19]. The grounding requirements of the casing will vary depending on the design of the equipment in use. However there are currently no guidelines defined for electrically bonding of composite materials. The effect that the number of bonding points has on the magnitude of the parameters in the lumped resistance model was investigated using the setup in Figure 6, in which copper foil was connected to the entry point and a chosen number of exit points. The copper foil at all exit points was then soldered on to a copper busbar, with the LCR meter measuring between the copper foil at the input, and copper busbar at the output. The dimensions of the electrodes were kept constant at 10mm x 10mm.

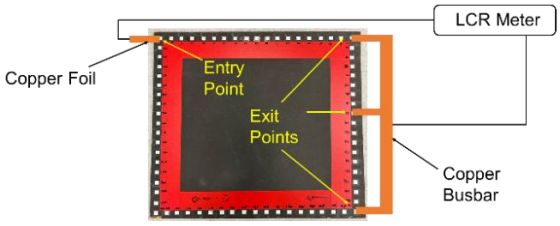

Figure 6: Experimental setup for investigation into number of bonding points

2. Experimentally captured parameters for lumped impedance model

The measured resistance for the variation in total resistance measured through the CFRP, with 10 x 10 mm electrodes, are shown in Figure 7. The variation of total resistance when electrodes are aligned in line with the carbon fibres in the top ply of the CFRP (blue) and when the electrodes are aligned perpendicular to the carbon fibres in the top ply of the CFRP (red) are both shown.

By inspection of Figure 7, when electrodes are aligned parallel to the fibres in the top ply and separated by a distance of less than 100 mm, resistance of the conducting pathway varies linearly with distance, and can be represented by

$$y = 2.939lx + 0.351 \quad (2),$$

where *lx (m)* is the distance between electrodes. The offset of 0.351 Ω can be attributed to the resistance as a result of the entry and exit points. When the distance between the electrodes is >100 mm, by inspection of Figure 7, the resistance increases at a much lower rate with distance, and can be expressed as:

$$y = 0.16lx + 0.671 \quad (3),$$

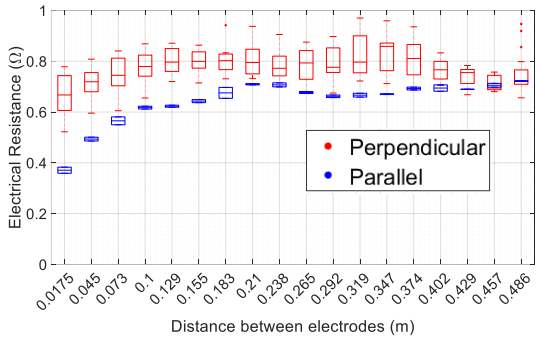

Figure 7: Resistance between 10 x10 mm electrodes for QI sample

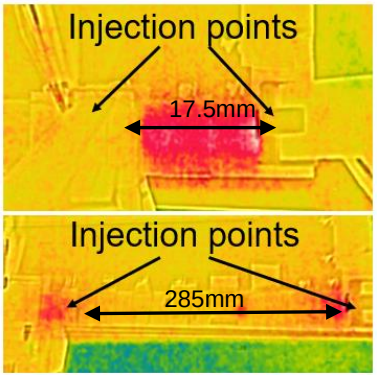

Figure 8: Thermal images of current conduction through CFRP

Figure 8 shows a thermal image of the surface of the CFRP when 3A is injected. By inspection of the thermal response, it is hypothesised that when electrodes are <100 mm apart the current is concentrated in the top ply of the CFRP for the full distance between the two electrodes. When electrodes are further apart, the current spreads out more through the full thickness and width of the CFRP.

It is important to note that for electrodes separated parallel to the top ply at distances greater than 100mm, the offset attributed to the entry and exit resistance has increased significantly from 0.351 Ω to 0651 Ω. It is hypothesised that as the distance between the electrodes increases, there are more connections between plies therefore increasing the number of parallel paths between the electrodes. As a result, the current must flow further into the CFRP at the entry and exit points, increasing *l* in (1), which will be in the direction of the thickness of the CFRP (z). Therefore, the resistance at the entry (or exit point) will increase. This increased entry and exit resistance will dominate the resistance of the pathway between the electrodes ($Rl_{x,y}$), reducing the influence of the distance between electrodes on the overall CFRP resistance. This hypothesis is supported by observations for UD [0º] material in [20].

By inspection of Figure 7, for electrodes separated perpendicular to the direction of the top ply of fibres sensitivity to distance is much less than for electrodes aligned with the direction of fibres in the top ply of CFRP. From the results gathered to date, the variation of resistance with distance can be expressed as

$$\boldsymbol{y = 0.0002ly + 0.670} \qquad (4),$$

where *ly (m)* is the distance between electrodes in the y-direction (perpendicular to direction of fibres on the surface of the CFRP). The higher offset resistance in (4) is attributed to the current at entry and exit points flowing a greater distance in the through thickness direction, than in the cases represented by (2) and (3).

Table 1: Lumped impedance models

Modelling Cases	**R_{entry}**	**R_{CFRP}**	**R_{exit}**
Case1: L<100mm, electrodes aligned parallel to top ply	0.1755Ω	$2.94L_x$	0.1755Ω
Case 2: L>100mm, electrodes aligned parallel to top ply	0.325 Ω	$0.0002L_x$	0.325 Ω
Case 3: Electrodes aligned perpendicular to top ply	0.335 Ω	$0.0002L_y$	0.335 Ω

The parameters for these three cases presented are summarised in Table 1. As the entry and exit electrode sizes are the same for each case, the entry (R_{entry}) and exit (R_{exit}) resistances, are assumed to be equal for each case, and hence the value of these is

half the value of the relevant offset resistance from (2), (3) or (4). Further work is needed to investigate the influence of electrodes being aligned diagonal to the top layer of carbon fibre plies.

3. Influence of electrode size and number on electrical resistance of CFRP

To enable the development of a set of design rules for CFRP casings for PEC modules for aircraft applications, an investigation into variation of the resistance through the CFRP was performed. This focussed on two areas, first the variation of resistance with electrode size, as the fault current injection area, due to abrasion, is expected to be smaller than 10 x 10 mm. Second, the influence of increased number of bonding points was investigated, as this may provide a route to tuning the resistance added by the CFRP to the fault current pathway.

Hence, the resistance between electrodes aligned with the direction of carbon fibre in the top ply was measured, for electrodes which were 2.5mm x 2.5mm, 5mm x 5mm and 10mm x 10mm. The results are shown in Figure 9. Table 2 compares the combined exit and entry resistances for the different electrode sizes. The data from Table 2 for the resistance of one electrode was plotted against cross-sectional area in Figure 11. By inspection, the relationship between the electrode size and resistance is given by:

$$\boldsymbol{R = 0.0004A^{-0.671}} \qquad (5)$$

Where *A* is the cross-sectional area of the electrode in m^2. This enables the resistance of a small cross-sectional entry point due to a chaffed wire to be estimated. This needs to be repeated for electrodes aligned perpendicular to the direction of carbon fibres, and results compared.

Second, the number of bonding points (exit points) was varied to investigate sensitivity of resistance the number of bonding points, the bonding points were separated from the entry point parallel to the orientation of the top ply of fibres, as shown in Figure 6. Figure 11 shows an exponential relationship between the electrical resistance and the number of bonding points, with the resistance becoming insensitive to the number of bonding points from 4 connections onwards.

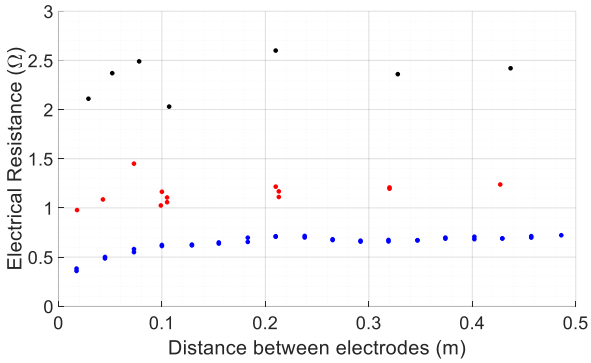

Figure 9: Change in resistance with variation in size of electrodes (blue: 10 x 10mm electrodes, red: 5 x 5mm electrodes, black: 2.5 x 2.5mm electrodes)

Table 2: Entry and exit resistance with dimensions of electrodes

Area of Electrodes (mm)	Entry + Exit Resistance	Electrode Resistance
10 x 10	0.351 Ω	0.1755 Ω
5 x 5	1.096 Ω	0.548 Ω
2.5 x 2.5	2.254 Ω	1.127 Ω

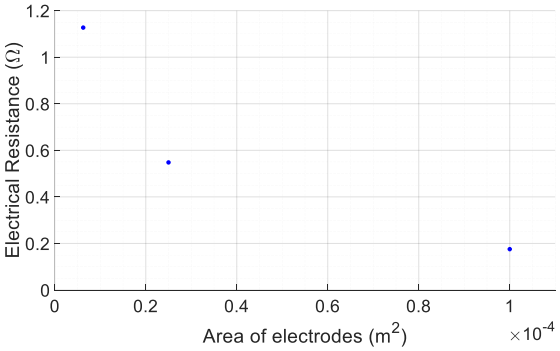

Figure 10: Electrical resistance corresponding to cross-sectional area of electrodes.

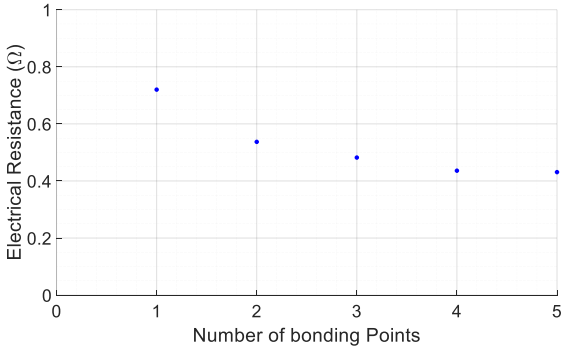

Figure 11: Variation in electrical resistance with increasing number of bonding points.

4. Rail to Ground Fault Analysis Through PEC CFRP Casing

4.1. Overview

To investigate the impact of the CFRP on fault response for a rail to ground fault through a CFRP casing, a model of the PEC module, with a 50-kVA motor load was built in Matlab Simulink. Figure 2 shows the subsystem which has been modelled, with an electrical fault thrown from phase A to ground on the output terminals of the PEC. The values for the current return network (CRN) are from [21]. It is expected that the most likely location for a rail to ground fault through the casing of the CFRP will be at the points where cables enter or exit the PEC module. Hence these may be AC or DC, and as such both an AC rail to ground and DC rail to ground fault was investigated. The threshold for fault detection according to [22] is a 30% increase above nominal current levels. Therefore, this investigation will determine if a fault through the CFRP to ground can be detected by traditional over-current fault detection methods.

The value R_{CFRP} is taken from the values from the experimental work presented in 3. Using the simulation model, the threshold resistance, $R_{threshold}$, was determined to be 4.1 Ω. Therefore, if the resistance added to the fault path by the CFRP exceed this value, the conventional over-current protection system deployed in the model will be unable to detect the fault, resulting in possible thermally induced damage to the casing. The fault response at the threshold resistance was compared with the fault response through an aluminium casing, in which the electrical resistance added to the fault path by an aluminium casing was calculated using (1), assuming a resistivity of 3.7×10^7 S/m, length of 100 mm and thickness of 4 mm. This is the same thickness as the CFRP used to populate the models, to enable comparison. In practice, thickness of the casing will be influenced by electro-magnetic shielding effectiveness requirements. However, this is out with the scope of this paper. The resistance of the aluminium casing was calculated to be 5.4 μΩ, this was then added to the maximum resistance permitted for an electrical bonding connection to ground (2.5 mΩ [17]), giving a total resistance for an aluminium casing of 2.51 mΩ.

Two further values for the resistance of the CFRP were also considered in this study. First the “best case” of fault resistance through CFRP, was estimated to be 0.7 Ω correlating to the value for the resistance in Figure 7, with a distance of more than 100 mm between entry and exit points, with an entry and exit cross-sectional area of 10 x 10 mm.

Finally, a “worst-case” electrical resistance was determined using the lumped impedance models for injection of electrical current through a very small cross-sectional area caused by the chaffing of a wire against the CFRP, causing the insulation to break down and expose the internal conductor to the CFRP surface. The entry resistance was calculated using (5), for a surface area of 1mm^2. This was calculated to be 4.24 Ω. The electrical resistance through the CFRP was calculated to be 0.1 Ω using (4), with the location of the electrical fault and the bonding point to ground separated by 500mm parallel to the orientation of the top ply of fibres. The resistance of the exit point was assumed to be 2.5 mΩ, corresponding with the maximum electrical resistance allowed for an electrical bonding point outlined in SAE-ARP-1870. Table 3 summarises the model parameters for the “worst-case” resistance for a fault through CFRP.

Table 3: Worst case electrical resistance through CFRP

R_{entry}	R_{CFRP}	R_{exit}	R_{total}
4.24 Ω	0.1 Ω	2.5 mΩ	4.34 Ω

4.2. Results

The results of the fault analysis of the PEC and CFRP casing are given in Figures 12-19. Figures 12 - 15 show the AC fault response and Figures 16-19 show the DC fault response for the resistances added to the fault path by the casing estimated in section 4.1.

4.3. Discussion of results

For the results of the AC faults in Figures 12 – 15, for the cases of “best-case” resistance of CFRP and the aluminium casing, when the fault occurs at 0.5 seconds the fault current through the casing exceeds the required 65 A to trip the protection system. However, for the “worst-case” electrical resistance through the CFRP casing the fault current through the casing did not exceed the required protection threshold, and the fault was unable to be detected with the over-current protection scheme. Further investigation is needed to determine methods to

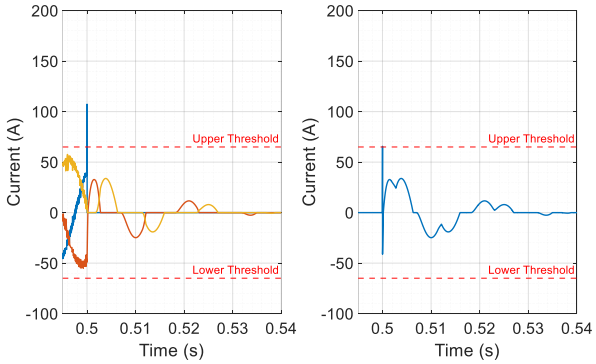

Figure 12: (Left) AC Phase currents during fault; (Right) Fault current through casing (fault resistance 4.1 Ω)

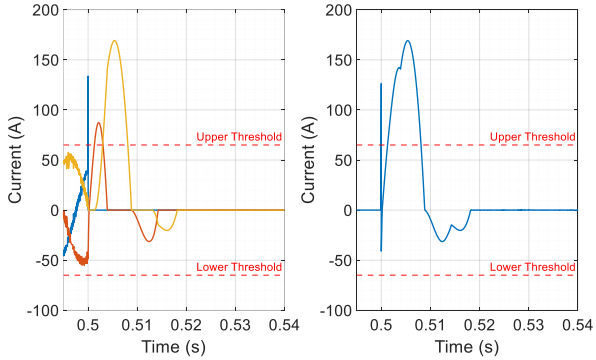

Figure 13: (Left) AC Phase currents during fault; (Right) Fault current through casing (fault resistance 2.5 mΩ)

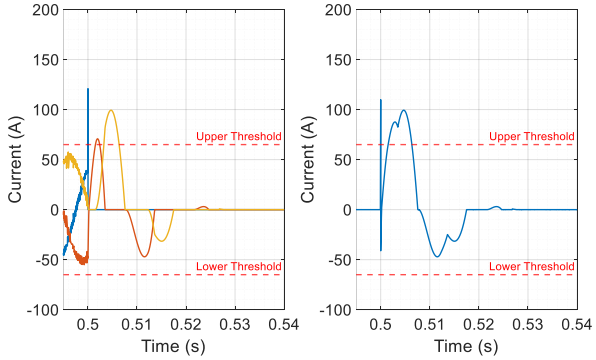

Figure 14: (Left) AC Phase currents during fault; (Right) Fault current through casing (fault resistance 0.7 Ω)

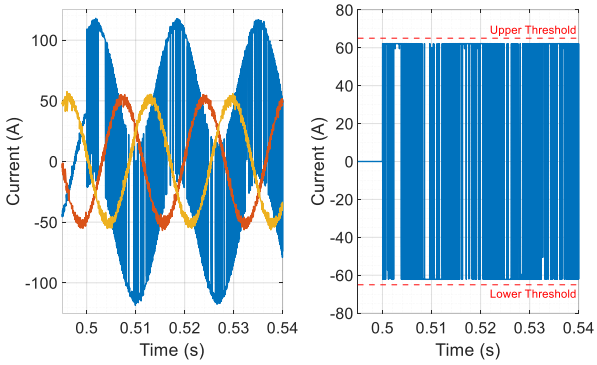

Figure 15: (Left) AC Phase currents during fault; (Right) Fault current through casing (fault resistance 4.34 Ω)

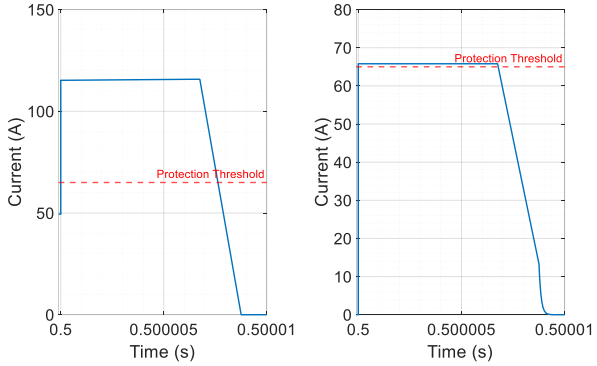

Figure 16: (Left) DC current during fault; (Right) Fault current through casing (fault resistance 4.1 Ω)

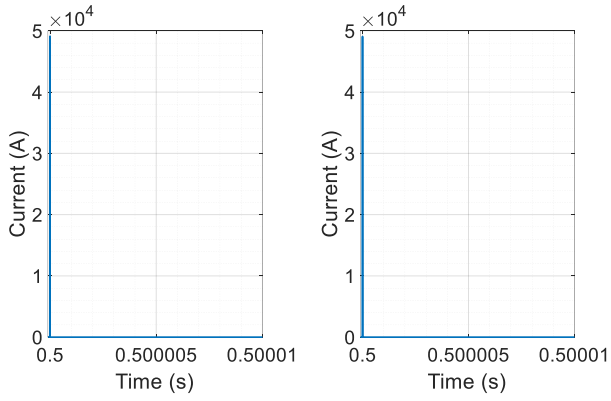

Figure 17: (Left) DC current during fault; (Right) Fault current through casing (fault resistance 2.5 mΩ) (Protection threshold at 65 A)

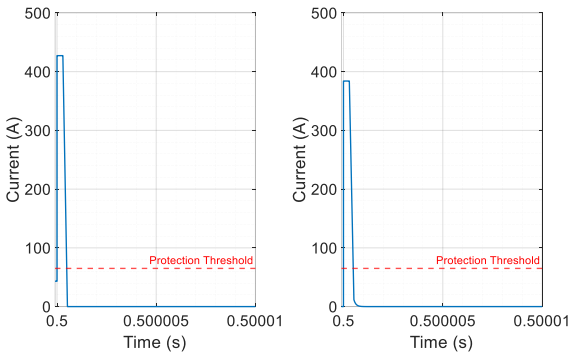

Figure 18: (Left) DC current during fault; (Right) Fault current through casing (fault resistance 0.7 Ω)

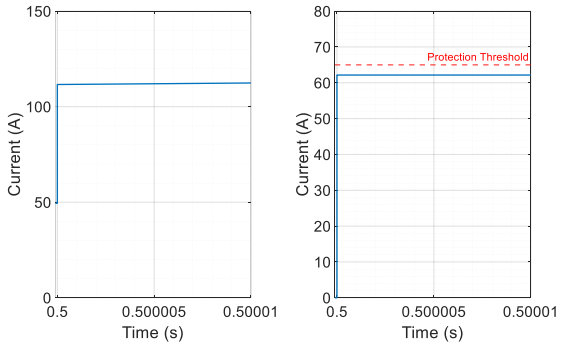

Figure 19: (Left) DC current during fault; (Right) Fault current through casing (fault resistance 4.34 Ω)

detect this fault. Second the AC fault results highlight a need to capture the thermal response of the CFRP to electrical fault current conduction, for all values of fault resistance, to fully determine the protection requirements. This was further underlined by examination of the DC fault results.

For the DC faults in Figures 16 -19, as the resistance increases, the time taken for the fault current to exceed the threshold for detection increases. The impact of the power dissipation during this period on the CFRP, in terms of damaging the CFRP, and determining the speed requirement of the protection, requires further investigation. When the resistance is above the threshold to trip the protection, the power dissipated at the entry point will be more than 14 kW. From previous studies of UD [0º], power dissipation of more than 20 W will result in the glass transition temperature of the resin being exceeded, and thermally induced degradation of the CFRP occurring.

The main factor impacting the total resistance added to the fault path by the CFRP is the cross-sectional area of the point at which the wire is chaffed against the CFRP surface. There are two areas for further investigation centred around this. The first to determine a realistic cross-sectional area for the entry point. Second, in the experimental work to capture the parameters for the models, silver paint electrodes were applied at both entry and exit points, as part of an established, experimental methodology from the literature to minimise contact resistance. However, in practice, there will be no electrode at the entry point into the CFRP for the fault current, only the exit where the casing is electrically bonded to ground. For two electrodes separated by 17.5mm, presented previously to be around 0.39 Ω for two electrodes of 10 mm x 10 mm, one electrode was removed and the resistance measured. The measured resistance increased to 16.53 Ω. This is well above the threshold resistance of 4.1 Ω for over-current fault detection in the case study in this paper.

Further investigation of the sensitivity to the total resistance to number of bonding points to ground on a panel is needed, to determine whether this offers a route to control fault resistance to be below a threshold value for detection. However, it is likely that the entry resistance will dominate the resistive pathway, and the impact of multiple bonding points to reduce the resistance of the CFRP will be minimal.

Conclusions

The experimentally derived lumped resistance models of CFRP enable the investigation of the influence of a CFRP casing around a PEC on the rail to ground fault response. The lumped resistance format of the models enable the influence of electrical bonding and characteristics of the injection site of the electrical fault current to be fully analysed. Most critically, this enables the estimation of power dissipation at different points in the fault current pathway through the CFRP, especially in cases where conventional over-current will not trip. The model also indicates that the impact of increasing number of bonding points, to reduce the resistance of the fault pathway through the CFRP is unlikely to be influential, due to the dominance of the resistance at the injection point.

The next stages for this work are to further extend the model to include injection sites without electrodes, and to subsequently design a set of experiments to capture the thermal and electrical response of the CFRP with time, to capture protection requirements. This data will enable the lumped impedance models to be developed into a set of time and temperature dependent models and integrated into the PEC model to give an accurate full system model. The final, full system model will enable low frequency design criteria for CFRP casings for PECs for aircraft applications.

References

1. Hall, C., et al. *Projecting Power Converter Specific Power Through 2050 for Aerospace Applications*. in *2022 IEEE Transportation Electrification Conference & Expo (ITEC)*. 2022.
2. Institute, A.T., *Electrical Propulsion Systems - Roadmap Report*. 2022.
3. Granger, M., et al., *Design of a High Power Density, High Efficiency, Low THD 250kW Converter for Electric Aircraft*. 2021.
4. Giglie, G., *Power Density Optimization Of EMI Filters For Power Electronic Converters*, in *Dipartimento di Energia, Ingegneria dell'Informazione e Modelli Matematici*. 2017, Universita Degli Studi Di Palermo.
5. *787 Dreamliner by design*. Available from: https://www.boeing.com/commercial/787/by-design/#/advanced-composite-use.
6. Aero Magazine, B., qtr_4, Chapter 4. *Boeing 787 from the ground up*. 2006; Available from: https://www.boeing.com/commercial/aeromagazine/srticles/qtr_04_06/article_04_2.html.
7. Zhao, Q., et al., *Review on the electrical resistance/conductivity of carbon fiber reinforced polymer*. APPL SCI-BASEL, 2019. **9**(11): p. 2390.
8. RTCA, *DO 160G Environmental conditions and test procedures for airbourne equipment*. 2014.
9. SAE, *Aircraft Electrical Power Systems Modelling and Simulation Definitions - AIR6326*. 2023.
10. Zhao, Q., et al., *Review on the Electrical Resistance/Conductivity of Carbon Fiber Reinforced Polymer*. Applied Sciences, 2019. 9(11).
11. Piche, A., et al., *Dynamic electrical behaviour of a composite material during a short circuit*. 2011. 128-132.
12. Piche, A., et al. *Numerical modeling support for the understanding of current distribution in carbon fibers composites*. in *2009 International Symposium on Electromagnetic Compatibility - EMC Europe*. 2009.
13. Senghor, F.D., et al., *Electrical Conductivity Tensor Modeling of Stratified Woven-Fabric Carbon Fiber Reinforced Polymer Composite Materials.* IEEE Transactions on Magnetics, 2017. 53(6): p. 1-4.
14. Jones, C.E., Johny, J., Norman, P., & Burt, G., *At scale, experimental capture of electrical response of carbon fibre composites to inform integrated electrical power and structural systems*, in *Paper presented at Towards Sustainable Aviation Summit 2022*. 2022: 3AF, Toulouse, France.
15. Jones, C.E., et al., *Electrical and Thermal Effects of Fault Currents in Aircraft Electrical Power Systems With Composite Aerostructures.* IEEE Transactions on Transportation Electrification, 2018. 4(3): p. 660-670.
16. Abry, J.C., et al., *In situ detection of damage in CFRP laminates by electrical resistance measurements.* Composites Science and Technology, 1999. 59(6): p. 925-935.
17. Aerospace, S. *Aerospace Recommended Practice 1870: Aerospace systems electrical bonding and grounding for electromagnetic compatibility and safety*. 2012.
18. Sierakowski, R.L., I.Y. Telitchev, and O.I. Zhupanska, *On the impact response of electrified carbon fiber polymer matrix composites: Effects of electric current intensity and duration.* Composites Science and Technology, 2008. 68(3): p. 639-649.
19. *IEEE Guide for Grounding of Instrument Transformer Secondary Circuits and Cases.* IEEE Std C57.13.3-2014 (Revision of IEEE Std C57.13.3-2005), 2015: p. 1-56.
20. Khan, J.B., et al., *Experimental electrical characterisation of carbon fibre*

composites for use in future aircraft applications. IET Science, Measurement & Technology, 2019. 13(8): p. 1131-1138.
21. Terörde, M., H. Wattar, and D. Schulz, *Phase Balancing for Aircraft Electrical Distribution Systems.* Aerospace and Electronic Systems, IEEE Transactions on, 2015. 51: p. 1781-1792.
22. Kaufmann, G. and R. Vaitkevičius, *Sensitive ground fault detection in compensated systems (arc suppression coil). What is influencing the sensitivity?* The Journal of Engineering, 2018. 2018(15): p. 971-977.